Frustrated crystallization of a monolayer of magnetized beads under geometrical confinement

J. Schockmel, N. Vandewalle, E. Opsomer, and G. Lumay
GRASP-CESAM, Physics Department, University of Liège, B-4000 Liège, Belgium
(Received 24 March 2017; published 15 June 2017)

We present a systematic experimental study of the confinement effect on the crystallization of a monolayer of magnetized beads. The particles are millimeter-scale grains interacting through the short range magnetic dipole-dipole potential induced by an external magnetic field. The grains are confined by repulsing walls and are homogeneously distributed inside the cell. A two-dimensional (2d) Brownian motion is induced by horizontal mechanical vibrations. Therefore, the balance between magnetic interaction and agitation allows investigating 2d phases through direct visualization. The effect of both confinement size and shape on the grains' organization in the low-energy state has been investigated. Concerning the confinement shape, triangular, square, pentagonal, hexagonal, heptagonal, and circular geometries have been considered. The grain organization was analyzed after a slow cooling process. Through the measurement of the averaged bond order parameter for the different confinement geometries, it has been shown that cell geometry strongly affects the ordering of the system. Moreover, many kinds of defects, whose observation rate is linked to the geometry, have been observed: disclinations, dislocations, defects chain, and also more exotic defects such as a rosette. Finally, the influence of confinement size has been investigated and we point out that no finite-size effect occurs for a hexagonal cell, but the finite-size effect changes from one geometry to another.

DOI: 10.1103/PhysRevE.95.062120

I. INTRODUCTION

For an infinite assembly of identical particles with isotropic interaction, the hexagonal lattice without defects represents the fundamental structure of a crystal. Topological defects play a key role in the study of the melting of two-dimensional (2d) systems [1–5], the propagation of cracks [6], the morphology of cell colonies [7], and the physical properties [8–11] of materials such as mechanical properties and electrical and thermal transport. Thus, controlling the number and the type of defects offers an interesting way to tune material properties. Curved surfaces, polydispersity, or geometrical confinement lead to the appearance of defects. Due to the large amount of biological and physical systems formed on curved backgrounds, the link between defects in 2d crystals and curved surfaces has been extensively studied, adopting two different points of view. On the one hand, the crystal is wrapped on a fixed curved surface (spheres, paraboloids, tori, and others), imposing defects [12–15]. On the other hand, defects are frozen in the crystal, inducing the buckling of the surface [16,17]. In flat geometry, defects are introduced with polydispersity [18] or with geometrical confinement. The study of the structure and the behavior of confined systems is motivated by the emergence of new technologies such as quantum dots [19,20] or hollow nanostructures [21–23].

Many studies have shown that the nature, the size, and the geometry of the spatial confinement can affect the dynamics of the system near the boundaries [24–26], the melting scenario [27–31], and the structure of the system [28–36]. In a previous study, with the same experimental setup [37], we have shown that a vibrated two-dimensional assembly of millimeter-scale grains interacting through a short range magnetic dipole-dipole potential can be used to study phase transitions. The macroscopic size of the grains allows a direct visualization of the dynamics. Moreover, we have shown that this macroscopic system mimics quantitatively colloidal suspensions [38]. In particular, the agitation was found to follow a Maxwellian distribution. The low-energy configuration of small systems, composed of a few dozen particles, is dominated by the geometry of the confinement, whether for a circular, square, hexagonal, or pentagonal geometry [31,33]. To our knowledge, only circular and hexagonal confinements have been studied for larger systems, composed of a few hundred particles [27,30,32,34–36].

In this paper, we present a systematic study of the effect of the confinement on the low-energy state of the system composed of a few hundred millimeter-scale grains, with magnetic dipole-dipole interaction, for triangular, square, pentagonal, hexagonal, heptagonal, and circular geometries with a homogeneous distribution of the particles.

II. EXPERIMENTAL SETUP

The experimental setup consists of a monolayer of N soft ferromagnetic spherical beads of diameter $d = 1$ mm and mass $m = 0.004$ g confined in a 2d horizontal cell with ferromagnetic walls. The beads are immersed in a vertical and homogeneous magnetic field H, produced by two 19 cm diameter coils in Helmholtz configuration, inducing magnetic dipole moments $\mu = V\chi_m H$ where V is the volume of the beads and the magnetic susceptibility $\chi_m = 3$ [39,40]. As the magnetic field is homogeneous and the beads are monodisperse, the repulsive potential between two beads separated by a distance r_{ij} can be written as

$$U_{ij} = \frac{\mu_0}{4\pi}\frac{V^2\chi_m^2 H^2}{r_{ij}^3}. \tag{1}$$

Thus the mean magnetic interaction energy between two beads is

$$\langle U\rangle = \frac{\mu_0}{4\pi}V^2\chi_m^2 H^2\left(\frac{\sqrt{3}}{2}\rho\right)^{3/2}, \tag{2}$$

 ©2017 American Physical Society

where ρ is the particle area density and $(\frac{2}{\sqrt{3}}\frac{1}{\rho})^{1/2}$ is the typical distance between two beads. The interactions are therefore well controlled by adjusting the strength of the external magnetic field H, ranging from 4900 to 11 800 A/m. Moreover, under an external magnetic field, the walls are repulsive and confine the beads. The cell is horizontally excited by two perpendicular electromagnetic shakers generating 35 Hz sinusoidal signals modulated by a white noise in amplitude. As shown in [37,38], this configuration leads to a 2d Brownian motion of the beads. The magnetic coupling parameter is defined as

$$\Gamma = \frac{\langle U \rangle}{\left\langle \frac{1}{2} m v^2 \right\rangle}. \tag{3}$$

The mean kinetic energy $\langle \frac{1}{2} m v^2 \rangle$ has been estimated with a 50 frames per second camera for $H = 4900$ A/m, because with such a value the magnetic interactions are weak and the agitation prevails. All experiments are fully controlled by a LABVIEW routine and follow the same protocol: for 2 seconds, a 11 800 A/m magnetic field is generated to spread homogeneously the set of beads in the cell. Simultaneously, the agitation is switched on and the magnetic field starts a linear increase from 4900 to 11 800 A/m for 200 seconds, corresponding to a slow cooling of the system from $\Gamma = 10$ to 70. Afterward, the magnetic field remains at its highest value for 30 seconds. This slow cooling allows the system to reach its stationary state, considered a crystal phase. Otherwise, the system would solidify in an amorphous state. The experimental protocol is the same for the complete set of experiments shown in the present paper. Two parameters are investigated: (i) the shape of the cell and (ii) the size of the cell. For each experiment, the filling fraction of the cell is fixed to $\phi = 0.24$ and the particle area density is $\rho = 315\,250$ beads per m^2. A CCD camera records a series of images at a fixed rate of 1 frame per second during the cooling process described above. The resolution of the camera in the region of interest is 500×500 pixels. The system is backlighted with a lattice of LEDs and a diffuser. Therefore, the beads and the background appear respectively in black and white. A basic analysis method allows us to determine the position of each bead during the whole process.

The numbers of beads chosen for the present study are $N = 169$, 331, and 721, satisfying the relationship giving the number of grains needed to fill a finite hexagonal lattice,

$$N = 3p^2 - 3p + 1, \tag{4}$$

where p is the number of beads on an edge.

III. RESULTS

A. Degree of ordering

The structural order of the system is characterized by the bond order parameter

$$\Psi_{6,i} = \frac{1}{n} \sum_{j=1}^{n} e^{i 6 \theta_{ij}}, \tag{5}$$

where the sum is carried out over the n nearest neighbors and θ_{ij} is the angle between the horizontal axis and the bond linking the particle i and its neighbor j. The modulus of the bond order parameter $|\Psi_{6,i}|$ gives information about the sixfold symmetry of the unit cell composed of the bead i and its first neighbors. Therefore $|\Psi_{6,i}| = 1$ when the unit cell follows a perfect sixfold symmetry, $|\Psi_{6,i}| < 1$ when the symmetry deviates from the perfect sixfold symmetry, and $|\Psi_{6,i}| = 0$ when the neighbors of the bead i are randomly orientated. The average over all the beads, excluding those near the walls, gives the global orientational order Ψ_6 of the system. One has

$$\Psi_6 = \langle |\Psi_{6,i}| \rangle. \tag{6}$$

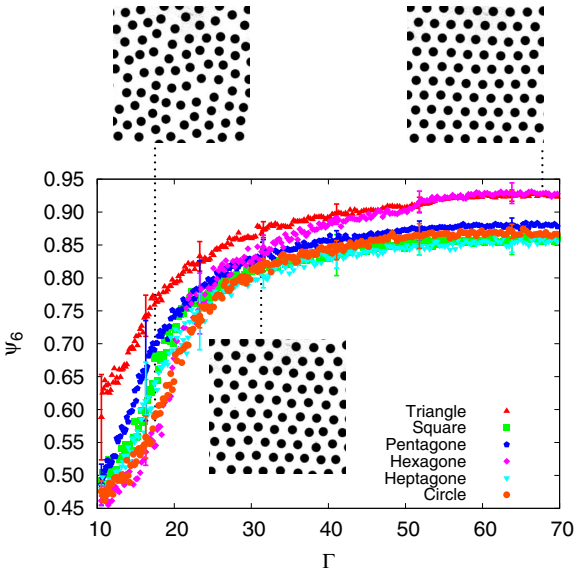

FIG. 1. Evolution of the global orientational order Ψ_6 during the 200 second cooling process for $N = 331$ beads. For each geometry of the cell, the points correspond to an average over three independent experiments. Typical error bars corresponding to the standard deviation are indicated.

The evolution of this global orientational order during the cooling process for $N = 331$ beads is reported in Fig. 1. For each cell geometry, the order parameter Ψ_6 saturates during the cooling, indicating that the maximum degree of order is achieved by the system. For each geometry, the final state of the system exhibits a global orientational order $\Psi_6 > 0.8$, ensuring that the system is in a crystalline state [41] and not trapped in an amorphous state.

The final value of Ψ_6 for each geometry is reported in Fig. 2. As expected, the final value of Ψ_6 for both triangular and hexagonal cell shapes is higher than the value obtained with other cell geometries. Indeed, the triangular and hexagonal cell shapes are compatible with the hexagonal lattice formed by the grain positions. Incompatibilities between cell shape and hexagonal lattice induce the presence of defects and reduce the global orientational order Ψ_6. The state reached by the system is not the ground state but a low-energy state. If the cell geometry is not compatible with the lattice, frustrations are created; these are a source of disorder leading to a competition between low-energy states. We show hereafter that this competition allows one to observe a wide range of defect types.

It has been checked that the equilibrium value of Ψ_6 is robust for a change in the filling fraction ϕ. For a variation

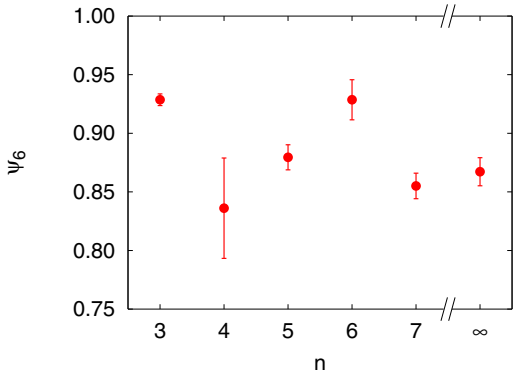

FIG. 2. Global bond order parameter Ψ_6 at the end of the cooling process as a function of the number n of edges of the cell. The error bars correspond to the standard deviation of ψ_6 over three independent experiments.

of ϕ from 0.20 to 0.28, the mean final values of Ψ_6 and their standard deviation are equivalent to those presented in Fig. 2.

B. Type and distribution of defects

Let us consider the nearest neighboring of each particle. The topological charge allocated to a particle i is defined as $Q_i = 6 - n_i$ for a particle belonging to the bulk and $Q_i = 4 - n_i$ for a particle at the boundary, where n_i corresponds to the coordination number of the particle i. The coordination number is determined using the Delaunay triangulation. The total topological charge of the system in a planar configuration must satisfy the Euler condition, i.e., $\sum_i^N Q_i = 6$. We checked that this condition is always satisfied in our system whatever the confinement geometry. Figure 3 shows snapshots of the system in the low-energy state for each geometry. The beads with sixfold ($Q = 0$), fivefold ($Q = 1$), and sevenfold ($Q = -1$) coordination numbers are respectively colored in yellow, red, and green in the Voronoi tessellation. Many types of defects have been observed in our system [34]. An isolated particle with a nonzero topological charge is called a disclination. A pair of fivefold and sevenfold disclinations is called a dislocation. Defect chains, also called grain boundaries, are alternating fivefold and sevenfold disclinations. These chains can be topologically neutral or charged. A scar is the most rudimentary defect chain, only composed of two fivefold and one sevenfold disclination. Most of the defects are observed as a chain with variable sizes or in the form of a topologically charged cluster. Figure 4 (left) shows a particularly well organized cluster with a $+1$ topological charge, called a rosette, with a fivefold symmetry. No neutral cluster have been observed. A topologically neutral defect is responsible of the loss of translational order and, according to the KTHNY (Kosterlitz, Thouless, Halperin, Nelson, and Young) theory [1–5], the topologically charged particles are responsible of the loss of orientational order. Thus, a charged defect tends to create curvature in crystal lines: $+1$ defects attract the lines of the lattice and -1 defects repel the lines of the lattice [13].

The observation probability of a topologically charged particle in the bulk belonging to a defect type, as described below, is reported in Table I. The defects are at least counted

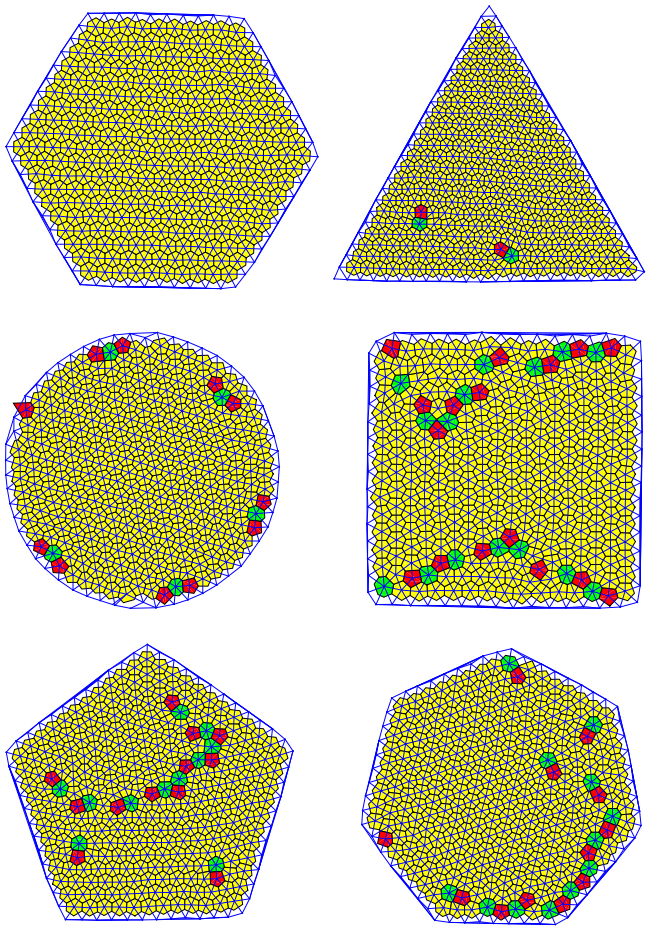

FIG. 3. Stack of Voronoi diagrams and Delaunay triangulations for each geometry with $N = 331$ beads. Beads with respectively fivefold, sixfold, and sevenfold coordination are colored in red, yellow, and green in the Voronoi diagram. Voronoi cells for beads at the boundary are not shown for clarity.

over 993 particles for each geometry. The cell geometry influences both the number and the distribution of defects among the different types listed. The mean number of topologically charged particles, $\langle N_D \rangle$, depends on the geometry of the confinement and can be directly related to Ψ_6.

We have observed that the cell geometry influences the spatial distribution of the defects in the system. Figure 5

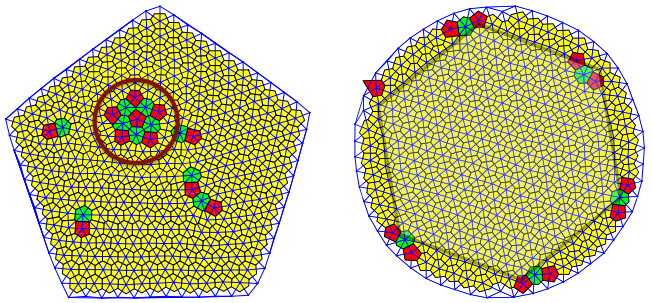

FIG. 4. (Left) Rosette defects in a pentagonal confinement. (Right) Six topologically charged defects near the boundary drawing a hexagon with the same orientation as the lattice.

TABLE I. Observation rate of a topologically charged particle in the bulk belonging to a dislocation, a disclination, a neutral chain, a charged chain, or a cluster for each geometry with an $N = 331$ beads system. $\langle N_D \rangle$ is the averaged number of topologically charged particles observed in an experiment. Counting is performed at least over three experiments.

	$\langle N_D \rangle$	Dislocation	Disclination	Neutral chain	Charged chain	Cluster	Rosette
Hexagon	0						
Triangle	6 ± 2	1.00	0.00	0.00	0.00	0.00	0.00
Circle	18 ± 4	0.04	0.00	0.00	0.96	0.00	0.00
Square	26 ± 11	0.22	0.07	0.28	0.20	0.23	0.00
Pentagon	19 ± 3	0.55	0.01	0.08	0.24	0.00	0.12
Heptagon	22 ± 2	0.46	0.06	0.24	0.24	0.00	0.00

presents the cumulated radial distribution of the topologically charged particle $N_D(r)$ for the final state of the system containing 331 beads for each geometry. Hexagonal and triangular cell geometries are not shown due to the lack of defects in these geometries. The cell geometry is found to affect significantly the radial distribution $N_D(r)$. In pentagonal cells, the defects are distributed everywhere in the cell, with the exception of the outer region containing only a few defects (mostly dislocations) which do not belong to a large chain or to a cluster. In contrast, all the defects in a circular cell are located in the outer region. Defects in squared or heptagonal cells are located everywhere but are more rare in the center. As shown by the cumulated radial distribution of the particle number $N(r)$ (see insert of Fig. 5), this difference is not explained by an inhomogeneity of the beads' distribution in the cell.

Since the selected bead number satisfies Eq. (4), almost no defects have been observed in the hexagonal cell, with the exception of rare dislocations because the system is not in the ground-state. Therefore, a nonzero probability to observe dislocation exists. In any case, the total topological charge in the bulk is $Q_{\text{bulk}} = 0$ and the defects at the boundary appear at the six corners of the cell.

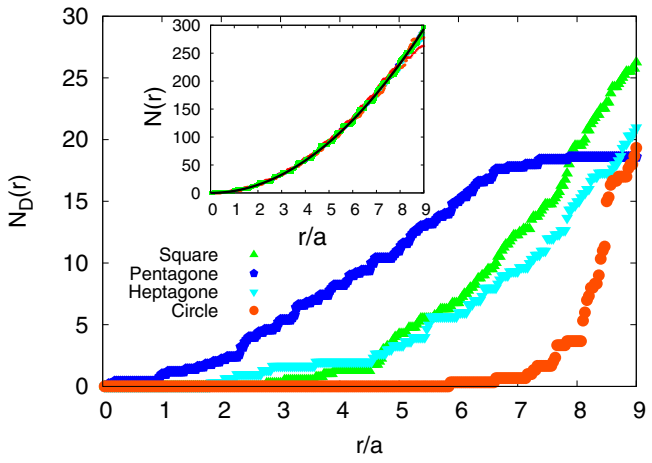

FIG. 5. Cumulated radial distribution of defects $N_D(r)$ for the final state of the system for square, pentagonal, heptagonal, and circular geometries for $N = 331$ beads. In the insert is the cumulated radial distribution of the particle number $N(r)$; the black curve corresponds to a homogeneous distribution. The distance r from the center is normalized by the mean distance a between two beads in the system.

Even if the triangular geometry is compatible with the hexagonal lattice, some dislocations are observed. Indeed, to fit a perfect hexagonal lattice in a triangular cell, the number of beads should follow the relation $N = p(p+1)/2$, which is not satisfied. As dislocations are topologically neutral, the total topological charge in the bulk is $Q_{\text{bulk}} = 0$ and two charged particles per corner are present at the boundary.

Crystals confined in a circular geometry have been widely studied, and our results are in agreement with the observations reported previously [27–29,32,34]. A monodomain crystal with hexagonal lattice is well defined in the bulk. Near the boundary, six defects with a $+1$ topological charge drawa hexagon with the same orientation than the lattice [see Fig. 4 (right)]. Unlike the hexagonal and triangular cells which fix the crystal orientation, the circular cell does not impose any privileged crystal orientation. For each independent experiments a random global orientation of the crystal is observed.

In the square cell, the orientation of the lattice is directed by two parallel edges among the four edges of the cell because the cell and the lattice are sharing a mirror symmetry. As a consequence, the defects are situated near the two frustrated edges and are aligned to form two grain boundaries. Despite these defects near the edges, we observe a large monodomain following a hexagonal lattice between the two grain boundaries, as illustrated in Fig. 3. In this geometry, the defect positions are well determined but the nature of the defects is diversified: dislocations and neutral and charged grain boundaries and clusters have similar occurrence probabilities. The global bond order parameter Ψ_6 is associated with a large error bar for a squared cell (see Fig. 2) because the structure of the system significantly changes from one experiment to an another, meaning that the square confinement represents a strong frustrat ion for a hexagonal cell.

For each experiment in the pentagonal cell, five topologically charged particles are found at the boundary at each corner of the cell. Therefore, the total topological charge in the bulk is $Q_{\text{bulk}} = +1$, in agreement with the Euler relation. Many neutral defects are observed, mainly dislocations, but no defects with negative topological charge are observed, meaning that only one defect with $+1$ topological charge is observed per experiment. This positive defects take the form of a positively charged chain of defects or can be a more exotic defect such as the rosette. As a consequence of the isolated charged defects in the bulk, the global orientation is decreased and the lattice appears distorted. Moreover, a long chain of defects situated in the middle of the bulk divides the

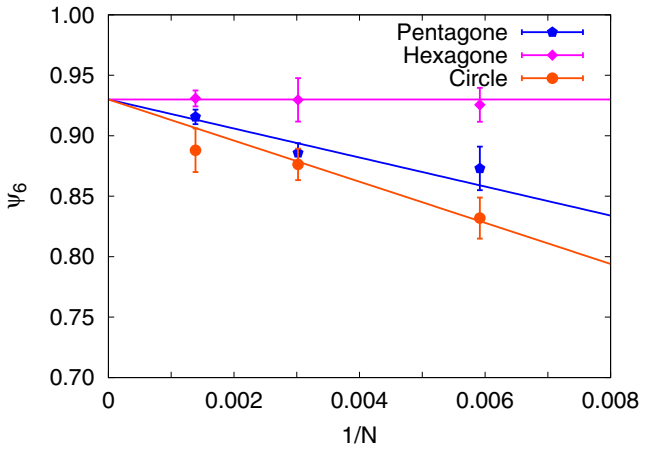

FIG. 6. Final value of Ψ_6 for pentagonal, hexagonal. and circular geometries for $N = 169$, 331, and 721 beads at constant filling fraction. The lines correspond to a linear fit.

crystal into two distinct domains with different orientations. In the other geometries, this phenomena is not observed because charged defects are in average located close to the boundaries or close to a defect with an opposite charge.

In the heptagonal cell, the observation of one positive boundary defect at each corner associated with a negative defect in the bulk could be expected. However, this defect distribution has not been observed. In all experiments, positive boundary defects are localized only at six of the seven cell corners, and the condition $Q_{\text{bulk}} = 0$ is always respected. Moreover, many dislocations are observed in the bulk. However, in each independent experiment with the heptagonal cell, we observe one positive defect and one negative defect separated by ten typical particle distances. Thus, as the two opposite charged defects are far from each other, a distortion in the lattice is observed.

C. Cell size effect

The effect of the confinement size has been studied. Figure 6 shows the final value of Ψ_6 for pentagonal, hexagonal, and circular geometries for $N = 169$, 331, and 721 beads with a constant filling fraction $\phi = 0.24$. The lines are guides for the eyes and correspond to linear fits for the hexagonal, pentagonal, and circular geometries. For each geometry, the final value of Ψ_6 converges to a unique value for large systems. Nevertheless, the finite size of the system affects the particle ordering.

As discussed in Sec. III B, the nature of the defects depends on the cell geometry. Therefore, it is not surprising to observe that the finite-size effect is different for hexagonal, pentagonal, and circular geometries. No finite-size effect is observed for the hexagonal confinement because this cell geometry induces the formation of a nearly perfect lattice. Indeed, the selected bead numbers $N = 169$, 331, and 721 are in agreement with Eq. (4).

The global order of the systems is more affected for small cell sizes in circular confinement than in pentagonal confinement because, in a curved boundary, the smaller the system is, the more the radius of curvature increases and prevents the hexagonal order.

IV. CONCLUSION

A model experimental set-p previously validated to study 2d phase transitions [37,38] has been used to perform a systematic study of the confinement effect on the crystallization of a monolayer of magnetized beads. The temperature is simulated by a mechanical agitation inducing Brownian motion of the beads. A slow cooling process from a liquid state to a solid state is used to reach the low-energy state of the system. We show that the geometry of the cell affects the type and the number of defects in the systems. In particular, the influence of both cell size and cell shape on the global bond order parameter Ψ_6 is analyzed. This order parameter is higher for triangular and hexagonal cells compared to squared, hexagonal, heptagonal, and circular shaped cells. Moreover, the order increases with the grain number N for constant filling fraction.

The type of defects (disclinations, dislocations, defect chains, and also more exotic defects such rosettes) and their occurrence have been analyzed for the different cell geometries. Only a few dislocations, that do not degrade significantly the ordering, are observed in hexagonal and triangular cells due to the compatibility between the grain lattice symmetry and the cell shape symmetry. Moreover, no finite-size effects are observed for these confinements. The other cell geometries (squared, hexagonal, heptagonal, and circular) display more complex defects modifying the ordering of the system. Topologically charged defects affect consequently the ordering of the system and destroy translational order as predicted by the KTHNY theory. Moreover, distortion in the system is observed if topologically charged defects are isolated in the bulk, and the long-sized defects tend to divide the system into different domains.

ACKNOWLEDGMENT

This work was financially supported by the FNRS (Grant PDR T.0043.14) and by the University of Liège (Starting Grant C-13/88).

[1] J. M. Kosterlitz and D. J. Thouless, J. Phys. C **6**, 1181 (1973).
[2] J. M. Kosterlitz, J. Phys. C **7**, 1046 (1974).
[3] B. I. Halperin and D. R. Nelson, Phys. Rev. Lett. **41**, 121 (1978).
[4] D. R. Nelson and B. I. Halperin, Phys. Rev. B **19**, 2457 (1979).
[5] A. P. Young, Phys. Rev. B **19**, 1855 (1979).
[6] M. J. Buehler, *Atomistic Modeling of Materials Failure* (Springer, New York, 2008).
[7] A. Doostmohammadi, S. P. Thampi, and J. M. Yeomans, Phys. Rev. Lett. **117**, 048102 (2016).
[8] Y. Wei, J. Wu, H. Yin, X. Shi, R. Yang, and M. Dresselhaus, Nat. Mater. **11**, 759 (2012).
[9] R. Grantab, V. B. Shenoy, and R. S. Ruoff, Science **330**, 946 (2010).
[10] O. V. Yazyev and S. G. Louie, Nat. Mater. **9**, 806 (2010).

[11] Z. Song, V. I. Artyukhov, B. I. Yakobson, and Z. Xu, Nano Lett. **13**, 1829 (2013).
[12] A. R. Bausch, M. J. Bowick, A. Cacciuto, A. D. Dinsmore, M. F. Hsu, D. R. Nelson, M. G. Nikolaides, A. Travesset, and D. A. Weitz, Science **299**, 1716 (2003).
[13] W. Irvine, V. Vitelli, and P. Chaikin, Nature (London) **468**, 947 (2010).
[14] N. A. Garcia, A. D. Pezzutti, R. A. Register, D. A. Vega, and L. R. Gomez, Soft Matter **11**, 898 (2015).
[15] F. L. Jimenez, N. Stoop, R. Lagrange, J. Dunkel, and P. M. Reis, Phys. Rev. Lett. **116**, 104301 (2016).
[16] E. H. Yong, D. R. Nelson, and L. Mahadevan, Phys. Rev. Lett. **111**, 177801 (2013).
[17] Z. Song, V. I. Artyukhov, J. Wu, B. I. Yakobson, and Z. Xu, ACS Nano **9**, 401 (2015).
[18] Z. Yao and M. Olvera de la Cruz, Proc. Natl. Acad. Sci. USA **111**, 5094 (2014).
[19] A. V. Filinov, M. Bonitz, and Y. E. Lozovik, Phys. Rev. Lett. **86**, 3851 (2001).
[20] M. Ishizuki, H. Takemiya, T. Okunishi, K. Takeda, and K. Kusakabe, Phys. Rev. B **85**, 155316 (2012).
[21] K. Koga, G. T. Gao, H. Tanaka, and X. C. Zeng, Nat. Lett. **412**, 802 (2001).
[22] Y. Sun, B. Mayers, T. Herricks, and Y. Xia, Nano Lett. **3**, 955 (2003).
[23] T. S. Ingebrigtsen, J. R. Errington, T. M. Truskett, and J. C. Dyre, Phys. Rev. Lett. **111**, 235901 (2013).
[24] L.-W. Teng, P.-S. Tu, and L. I, Phys. Rev. Lett. **90**, 245004 (2003).
[25] K. Watanabe, T. Kawasaki, and H. Tanaka, Nat. Mater. **10**, 512 (2011).
[26] A. Schella, A. Melzer, C. July, and C. Bechinger, Soft Matter **11**, 1197 (2015).
[27] Y.-J. Lai and L. I, Phys. Rev. E **64**, 015601(R) (2001).
[28] M. Kong, B. Partoens, and F. M. Peeters, Phys. Rev. E **67**, 021608 (2003).
[29] M. Kong, B. Partoens, A. Matulis, and F. M. Peeters, Phys. Rev. E **69**, 036412 (2004).
[30] V. M. Bedanov and F. M. Peeters, Phys. Rev. B **49**, 2667 (1994).
[31] T. O. E. Skinner, H. M. Martin, D. G. A. L. Aarts, and R. P. A. Dullens, Soft Matter **9**, 10586 (2013).
[32] A. A. Koulakov and B. I. Shklovskii, Phys. Rev. B **57**, 2352 (1998).
[33] R. Bubeck, S. Neser, C. Bechinger, and P. Leiderer, Prog. Colliod Polym. Sci. **110**, 41 (1998).
[34] A. Radzavilavicius and E. Anisimovas, J. Phys.: Condens. Matter **23**, 385301 (2011).
[35] Z. Yao and M. Olvera de la Cruz, Phys. Rev. Lett. **111**, 115503 (2013).
[36] I. Williams, E. C. Oguz, R. L. Jack, P. Bartlett, H. Löwen, and C. P. Royall, J. Chem. Phys. **140**, 104907 (2014)
[37] J. Schockmel, E. Mersch, N. Vandewalle, and G. Lumay, Phys. Rev. E **87**, 062201 (2013).
[38] R. Messina, S. Aljawahri, L. Bècu, J. Schockmel, G. Lumay, and N. Vandewalle, Sci. Rep. **5**, 10348 (2015).
[39] S. Merminod, M. Berhanu, and E. Falcon, Europhys. Lett. **106**, 44005 (2014).
[40] S. Merminod, T. Jamin, E. Falcon, and M. Berhanu, Phys. Rev. E **92**, 062205 (2015).
[41] P. M. Reis, R. A. Ingale, and M. D. Shattuck, Phys. Rev. Lett. **96**, 258001 (2006).